Temperature dependent TAPO model for failure analysis of adhesively bonded joints due to temperature induced manufacturing and service loading

P. Kühlmeyer and A. Matzenmiller, Institute of Mechanics, University of Kassel

In this contribution, the focus of the material model is to predict failure of joints, which are bonded with ductile-modified adhesives and subjected to manufacturing and service loading with low strain rates during and after cure due to temperature changes. Therefore, a linear thermo-viscoelastic model is arranged in series to the Toughened Adhesive Polymer (TAPO) model. By reason of numerical efficiency, the equations of the TAPO model are reduced to the cohesive zone theory and implemented into LS-DYNA as a “user defined cohesive model” assuming a thin adhesive layer between the adherends. The parameters of the constitutive equations are identified by Dynamic Mechanical Analysis and by fitting the model response to data of shear tests using the thick adherend shear specimen (TASS) and tension tests by means of the butt joint specimen (BJS) conducted within the range from ambient temperature to nearly glass transition and from uncured up to fully cured adhesive.

1 Introduction

In modern light weight design, various materials with different physical properties are assembled to large structures, e.g. car body or aircraft fuselage. One common joining technology is adhesive bonding, which allows combining a wide range of different materials, e.g. various metals, carbon fibre composites, and polymers. As a consequence, the adhesive bonding technique is adopted by many branches, as for instance the automotive, and the aircraft industry. Vastly loaded structures are bonded with so called high-strength structural adhesives exhibiting high tensile strength and ductility. These properties are achieved by modifying the epoxy resin with rubber particles to improve the persistency and energy absorption until failure. The mechanical properties of structural adhesives are generally influenced by deformation, temperature, stress or its rates as well as the degree of polymerisation (cross-linking). So, the design of structures becomes more complicated and cost-intensive, if such adhesives are used. Hence, simulation with the Finite Element Method (FEM) is an efficient way to reduce costs in the development process within the framework of computer-aided design. Though, constitutive models are necessary for the prediction of the material behaviour under various loading conditions by means of the Finite Element (FE) analysis. In this context, the development of phenomenological constitutive models becomes very important for the simulation of adhesively bonded joints.

Recently, the so-called **T**oughened **A**dhesive **Po**lymer (TAPO) model has been made available in LS-DYNA for solid elements. The TAPO equations describe the mechanical behaviour of structural adhesives under crash conditions by taking elasticity, viscoplasticity and damage due to plastic deformation into account—see [1], pp. 69–90, [2], pp. 250–282, [3], pp. 54–69, and [4], pp. 2-1152-2-1158. It was developed by the Institute of Mechanics (IfM) at the University of Kassel in both research projects with the grant numbers P 676 [1] and P 828 [2] of the Forschungsvereinigung Stahlanwendung e.V. (FOSTA). Also, the TAPO model is applicable for the cohesive elements with an option in LS-DYNA reducing the kinematics of the continuum to the local displacement jump as shown in [2], p. 288, [3], p. 113, and [5]. In addition, the constitutive equations of the TAPO model are reduced to the interface theory for cohesive elements in [3], pp. 106 ff. The interface theory is applied to the failure prediction of adhesively bonded joints with thin adhesive layers in [5] to [8]. Furthermore, the numerical efficiency of the cohesive element in the framework of the FEM is discussed in [8].

As outlined in [1] to [8], the constitutive models are applied to predict failure of bonded structures under crash conditions. Recently, the simulation of adhesively bonded joints focuses also on manufacturing and service processes—see [9] and [10]. The influence of the temperature course on the material behaviour is important for the design of adhesively bonded structures, whereas the entire temperature-time history is fundamental for the polymerisation of the thermosetting resins. Especially, the thermo-viscoelastic properties of ductile-modified adhesives must be account for in stress levels below and beyond the yield strength.

This contribution concerns with the constitutive modelling of the temperature influence on thermosetting, ductile-modified adhesives during cross-linking. The present investigations focuses on the long-term behaviour of the adhesive bond in bimetallic structures, undergoing temperature induced loadings due to the uneven expansions caused by different thermal expansion coefficients of the adherends. So, the reduced TAPO model in [3] is extended to temperature and cure dependent viscoelasticity, plasticity and damage, considering rate, temperature and curing effects below and beyond the yield strength.

The constitutive model and its consistent tangent modulus are implemented for the quasi-static FE analysis into the code of LS-DYNA to simulate the long-term behaviour of adhesive bonds. The material model is suited to predict failure of adhesively bonded joints beyond the gelification point for manufacturing and service loading due to evolving temperature courses.

2 Thermo-chemo-viscoelastic-plastic model with ductile damage

The thin structural adhesive layer of a joint is modelled as an interface between the adherends assuming zero thickness in the model. Hence, an interfacial constitutive model (cohesive zone) is proposed including thermo- and chemo-viscoelasticity, -plasticity, and a ductile damage approach. The viscoelastic, thermal, and plastic contributions in the constitutive model are shown as a serial arrangement of related bodies in the rheological network in Fig. 1. On the left hand side, the generalised MAXWELL body represents the viscoelastic material properties of the adhesive with different parallel chains of springs and dashpots to describe the overstress and one parallel spring to account for the equilibrium stress in the normal and tangential direction of the interface. The material parameters k_i and g_i are the stiffness parameters of the springs whereas the constants $\hat{\tau}_i^{\mathrm{n,s}}$ are the relaxation times in the MAXWELL chains, while k_∞ and g_∞ are the stiffness parameters for the equilibrium state. The thermal strain element is connected in series to the MAXWELL model in order to describe the thermal expansion and the chemical shrinkage of the adhesive layer as a thermo-chemical displacement jump in normal direction $\boldsymbol{\Delta}^{\mathrm{tc}} = \boldsymbol{\Delta}^{\mathrm{th}} + \boldsymbol{\Delta}^{\mathrm{ch}}$. The rate of the thermal displacement is proportional to the temperature change $\dot{\theta}$ and the adhesive layer thickness d_{k} with the unit vector normal to the interface $\mathbf{e}_{\mathrm{n}} = \{1 \quad 0 \quad 0\}^{\mathrm{T}}$ and the thermal expansion coefficient $\tilde{\alpha}_{\mathrm{th}}$.

$$\dot{\boldsymbol{\Delta}}^{\mathrm{th}} = \tilde{\alpha}_{\mathrm{th}}\, d_{\mathrm{k}}\, \dot{\theta}\, \mathbf{e}_{\mathrm{n}} \tag{1}$$

The thermal expansion coefficient $\tilde{\alpha}_{\mathrm{th}}$ changes at the glass transition temperature θ_{g} and depends on the degree of cure p as in [10], p. 85.

$$\tilde{\alpha}_{\mathrm{th}} = \begin{cases} \alpha_1 & \text{if} \quad \theta < \theta_{\mathrm{g}} \\ \alpha_2 + (\alpha_3 - \alpha_2)(1-p) & \text{if} \quad \theta \geq \theta_{\mathrm{g}} \end{cases}$$

The chemical displacement $\boldsymbol{\Delta}^{\mathrm{ch}}$ is postulated as

$$\boldsymbol{\Delta}^{\mathrm{ch}} = \frac{d_{\mathrm{k}}}{3}\left(\beta_2\, p - \beta_1\, p^2\right) \mathbf{e}_{\mathrm{n}} \tag{2}$$

following [10], p. 93, Eq. (6.22) with the material parameters β_1 and β_2. On the right hand side, the TAPO model is represented by the friction element of ST-VENANT with the yield threshold $\tau_{\theta\mathrm{c}}$ and the spring with the parameters H_θ, q_θ, and b_θ, describing nonlinear isotropic hardening. Here, the TAPO model is active only when the adhesive changes its phase from liquid to solid (gelation) irreversibly—see [11]. The rheological network directly provides the additive split of the local, total displacement jump $\boldsymbol{\Delta}$ into the viscoelastic, thermal and plastic contribution:

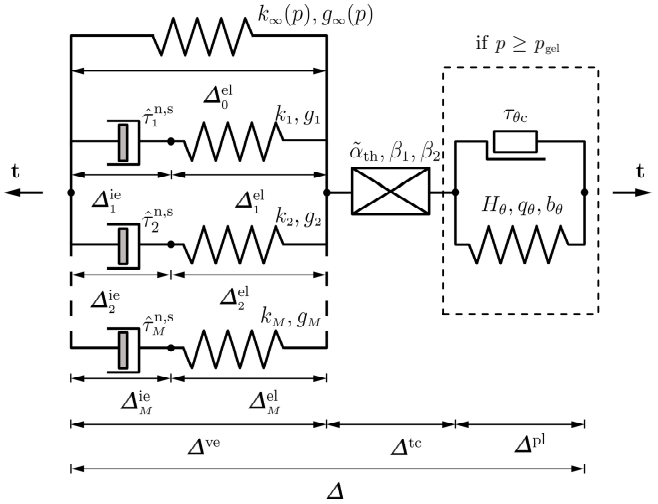

Fig. 1 Rheological network of constitutive model

$$\boldsymbol{\Delta} = \boldsymbol{\Delta}^{\mathrm{ve}} + \boldsymbol{\Delta}^{\mathrm{th}} + \boldsymbol{\Delta}^{\mathrm{pl}} \tag{3}$$

2.1 Thermo-chemo-viscoelastic constitutive model

The interface traction $\mathbf{t}$ is postulated as a functional of the viscoelastic displacement jump $\boldsymbol{\Delta}^{\mathrm{ve}}$. Its constitutive parameters are a function of the temperature $\theta(t)$ and the degree of cure $p(t)$ changing in time t.

$$\mathbf{t}(t) = \boldsymbol{\mathcal{F}}_{\tau \leq t}\left\{\boldsymbol{\Delta}^{\mathrm{ve}}(\tau); \tau, t\right\} \tag{4}$$

with the time variables t and τ—see [9], p. 177, Eq. (6.4).

The degree of cure p is defined as a scalar variable, which is $p = 0$ for the unlinked and $p = 1$ for the completely cross-linked polymer, $p \in [0,1]$. It is modelled with an implicit, nonlinear evolution equation of the KAMAL and SOUROUR type depending on the temperature course in time as follows—cf. [12] and [13]:

$$\dot{p} = A_1(\theta)(1-p)^{n_1} + A_2(\theta) p^m (1-p)^{n_2} \tag{5}$$

with the material parameters m, n_1, n_2 and the ARRHENIUS equations $A_1(\theta)$ and $A_2(\theta)$

$$A_1(\theta) = A_{10} \exp\left(-\frac{E_1}{R\,\theta}\right), \quad A_2(\theta) = A_{20} \exp\left(-\frac{E_2}{R\,\theta}\right), \tag{6}$$

with the pre exponential factors A_{10} and A_{20} as well as the activation energies E_1 and E_2 and the universal gas constant $R = 8.3144598\,\mathrm{J}/\mathrm{mol\,K}$.

A thermo- and chemorheologically simple material behaviour is assumed for the sake of temperature and cure dependent relaxation times—see [14], [15], pp. 266 ff, [16], pp. 202 ff, [17], and [18]. Due to the time-temperature and time-cure shift, all relaxation times $\hat{\tau}_i^{\mathrm{n,s}}$ are described with two functions of temperature for the normal (n) and tangential (s) direction of the interface $a_{\mathrm{T}}^{\mathrm{n}}(\theta)$ and $a_{\mathrm{T}}^{\mathrm{s}}(\theta)$ as well as one function depending on the degree of cure $a_{\mathrm{c}}(p)$. These functions are known as shift functions—see e.g. [19], pp. 94 ff. Furthermore, the reduced times ξ_{n} and ξ_{s} are introduced, which are determined by time integrals with the empirical shift functions

$$\xi_{\mathrm{n}}(t) = \int_0^t \frac{\mathrm{d}s}{a_{\mathrm{T}}^{\mathrm{n}}\left(\theta(s)\right) a_{\mathrm{c}}^{\mathrm{s}}\left(p(s)\right)}, \qquad \xi_{\mathrm{s}}(t) = \int_0^t \frac{\mathrm{d}s}{a_{\mathrm{T}}^{\mathrm{s}}\left(\theta(s)\right) a_{\mathrm{c}}^{\mathrm{s}}\left(p(s)\right)}, \tag{7}$$

to take into account the influence of the temperature course $\theta(t)$ and the degree of cure $p(t)$ on the relaxation times through the time scale. The time-temperature shift functions consist of an ARRHENIUS-typ equation for temperatures below the reference temperatures $\theta_{\mathrm{R}}^{\mathrm{n}}$ and $\theta_{\mathrm{R}}^{\mathrm{s}}$ and the WILLIAMS-LANDEL-FERRY equation [20] for temperatures beyond the reference level:

$$a_{\mathrm{T}}^{\mathrm{n,s}}(\theta) = \begin{cases} \exp\left[E_{\mathrm{A}}^{\mathrm{n,s}}\left(\dfrac{1}{\theta} - \dfrac{1}{\theta_{\mathrm{R}}^{\mathrm{n,s}}}\right)\right] & \text{if} \quad \theta < \theta_{\mathrm{R}}^{\mathrm{n,s}} \\ \exp\left[-\dfrac{C_1^{\mathrm{n,s}}\left(\theta - \theta_{\mathrm{R}}^{\mathrm{n,s}}\right)}{C_2^{\mathrm{n,s}} + \theta - \theta_{\mathrm{R}}^{\mathrm{n,s}}}\right] & \text{if} \quad \theta \geq \theta_{\mathrm{R}}^{\mathrm{n,s}} \end{cases} \tag{8}$$

with the material parameters $E_{\mathrm{A}}^{\mathrm{n,s}}$, $C_1^{\mathrm{n,s}}$, and $C_2^{\mathrm{n,s}}$. For the time-cure-shift, functions $a_{\mathrm{c}}^{\mathrm{n,s}}(p)$ are proposed by EOM et al. [21] consisting of an ansatz below and one beyond the gelification of the adhesive as follows:

$$a_{\mathrm{c}}^{\mathrm{n,s}}(p) = \begin{cases} \exp\left(-a_{\mathrm{gel}}^{\mathrm{n,s}}\left(a_1^{\mathrm{n,s}}\right)^{(p-p_{\mathrm{gel}})}\left(\dfrac{1-p}{1-p_{\mathrm{gel}}}\right)^{a_2^{\mathrm{n,s}}}\right) & \text{if } p \geq p_{\mathrm{gel}} \\ \exp\left(a_3^{\mathrm{n,s}}\,(p - p_{\mathrm{gel}}) - a_{\mathrm{gel}}^{\mathrm{n,s}}\right) & \text{if } p < p_{\mathrm{gel}} \end{cases} \tag{9}$$

Here, the reference of the time-cure shift functions $a_{\mathrm{c}}^{\mathrm{n,s}}(p)$ is the degree of cure for gelification p_{gel} (gel point) and the material parameters are the shifts at the gel point $a_{\mathrm{gel}}^{\mathrm{n,s}}$ as well as the parameters $a_1^{\mathrm{n,s}}$, $a_2^{\mathrm{n,s}}$ and $a_3^{\mathrm{n,s}}$.

The viscoelastic traction is written as a convolution integral over the viscoelastic displacement jump $\boldsymbol{\Delta}^{\mathrm{ve}}$ with the kernel functions R_{n} and R_{s} in the normal and tangential direction of the interface as follows:

$$\begin{aligned} \mathbf{t} = &\left[\int_{-\infty}^{t} k_\infty(p)\frac{\mathrm{d}\Delta_{\mathrm{n}}^{\mathrm{ve}}}{\mathrm{d}\tau}\mathrm{d}\tau + \int_{-\infty}^{\xi_{\mathrm{n}}(t)} R_{\mathrm{n}}(\xi_{\mathrm{n}}(t)-\tau)\frac{\mathrm{d}\Delta_{\mathrm{n}}^{\mathrm{ve}}}{\mathrm{d}\tau}\mathrm{d}\tau\right]\mathbf{e}_{\mathrm{n}} \\ &+\left[\int_{-\infty}^{t} g_\infty(p)\frac{\mathrm{d}\Delta_{\mathrm{t}}^{\mathrm{ve}}}{\mathrm{d}\tau}\mathrm{d}\tau + \int_{-\infty}^{\xi_{\mathrm{s}}(t)} R_{\mathrm{s}}(\xi_{\mathrm{s}}(t)-\tau)\frac{\mathrm{d}\Delta_{\mathrm{t}}^{\mathrm{ve}}}{\mathrm{d}\tau}\mathrm{d}\tau\right]\mathbf{e}_{\mathrm{t}} \\ &+\left[\int_{-\infty}^{t} g_\infty(p)\frac{\mathrm{d}\Delta_{\mathrm{b}}^{\mathrm{ve}}}{\mathrm{d}\tau}\mathrm{d}\tau + \int_{-\infty}^{\xi_{\mathrm{s}}(t)} R_{\mathrm{s}}(\xi_{\mathrm{s}}(t)-\tau)\frac{\mathrm{d}\Delta_{\mathrm{b}}^{\mathrm{ve}}}{\mathrm{d}\tau}\mathrm{d}\tau\right]\mathbf{e}_{\mathrm{b}} \end{aligned} \tag{10}$$

Both, the traction vector, $\mathbf{t} = \{t_{\mathrm{n}} \quad t_{\mathrm{t}} \quad t_{\mathrm{b}}\}^{\mathrm{T}}$, and the displacement jump vector, $\boldsymbol{\Delta} = \{\Delta_{\mathrm{n}} \quad \Delta_{\mathrm{t}} \quad \Delta_{\mathrm{b}}\}^{\mathrm{T}}$, act in normal, tangential, and binormal direction of the interface. According to [22], p. 60, Eq. (3.3-4), the kernel functions R_{n} and R_{s} are decoupled. From the rheological network of linear springs and NEWTON dashpots in Fig. 1, the functions R_{n} and R_{s} follows as DIRICHLET-PRONY series for a total of M MAXWELL elements for the normal and each shear component:

$$R_{\mathrm{n}} = \sum_{i=1}^{M} k_i \exp\left(-\frac{\xi_{\mathrm{n}}(t)}{\hat{\tau}_i^{\mathrm{n}}}\right), \; R_{\mathrm{s}} = \sum_{i=1}^{M} g_i \exp\left(-\frac{\xi_{\mathrm{s}}(t)}{\hat{\tau}_i^{\mathrm{s}}}\right) \tag{11}$$

In R_{n} and R_{s}, the equilibrium stiffness k_∞ and g_∞ are functions of the degree of cure p written as

$$k_\infty = \hat{k}_\infty \left(\frac{\left\langle p^2 - {p_{\mathrm{gel}}}^2 \right\rangle}{1 - {p_{\mathrm{gel}}}^2}\right)^{\frac{8}{3}}, \; g_\infty = \hat{g}_\infty \left(\frac{\left\langle p^2 - {p_{\mathrm{gel}}}^2 \right\rangle}{1 - {p_{\mathrm{gel}}}^2}\right)^{\frac{8}{3}}, \tag{12}$$

with the stiffness $\hat{k}_\infty$ and $\hat{g}_\infty$ of the fully cured adhesive for $p = 1$ as proposed by ADOLF and MARTIN in [17] and [18].

2.2 Temperature and cure dependent TAPO interface constitutive model

The scalar damage variable D is introduced to describe isotropic damage in the adhesive layer. The definition of damage is based on KACHANOV [23] as the ratio of the damaged to the initial cross section area A_{d} and A_0, respectively—see Fig. 2. It is considered in the equations of the constitutive model by using the concept of effective stress as in RABOTNOV [24]. Here, the nominal traction vector $\mathbf{t}$ in the convolution integral (10) is related to the effective traction vector $\hat{\mathbf{t}}$ according to RABOTNOV's proposal:

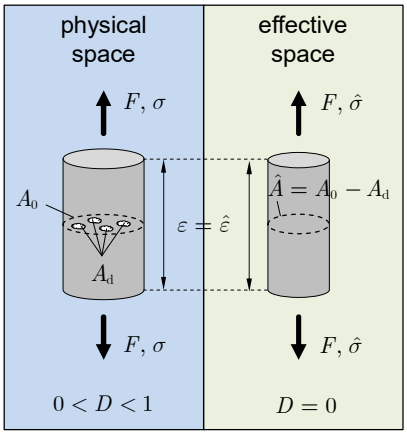

Fig. 2 Motivation of damage and concept of effective stresses

$$\hat{\mathbf{t}} = \frac{\mathbf{t}}{1-D} \qquad \text{with} \qquad D = \frac{A_{\mathrm{d}}}{A_0} \tag{13}$$

In addition, the strain equivalence principle is assumed, which postulates the equality of the strains for the damaged nominal state (physical space) and the undamaged effective state (effective space), $\varepsilon = \hat{\varepsilon}$ as shown in Fig. 2. As a consequence, it leads to the equality of all internal variables of the strain-type, for example $\varepsilon^{\mathrm{pl}} = \hat{\varepsilon}^{\mathrm{pl}}$—see e.g. [25]. In the TAPO cohesive zone model, the interfacial yield function $\tilde{f}$ depends on the normal component $\hat{t}_{\mathrm{n}}$ and the resultant shear stress $\hat{\tau} = \sqrt{\hat{t}_{\mathrm{t}}^{\,2} + \hat{t}_{\mathrm{b}}^{\,2}}$ of the effective interface traction $\hat{\mathbf{t}}$ as well as the yield stress τ_{y} and the yield threshold $\tau_{\theta\mathrm{c}}$ in Eq. $(14)_1$. In addition, the plastic potential $\tilde{f}^*$ $(14)_2$ is presented for a non-associated flow rule to avoid the evolution of normal plastic displacement jump $\Delta_{\mathrm{n}}^{\mathrm{pl}}$ during a simple shear process.

$$\begin{aligned} \tilde{f} &= \hat{\tau}^2 + \tilde{a}_1\,\tau_{\theta\mathrm{c}}\,\hat{t}_{\mathrm{n}} + \tilde{a}_2\left\langle \hat{t}_{\mathrm{n}} \right\rangle^2 - {\tau_{\mathrm{y}}}^2\,, \\ \tilde{f}^* &= \hat{\tau}^2 + \tilde{a}_2^*\left\langle \hat{t}_{\mathrm{n}} \right\rangle^2 - {\tau_{\mathrm{y}}}^2 \end{aligned} \tag{14}$$

Both functions are defined by using the MACAULEY bracket $\langle x \rangle = (\mathrm{x} + |\,\mathrm{x}\,|)/2$ to obtain asymmetric functions in tension ($\hat{t}_\mathrm{n} \geq 0$) and compression ($\hat{t}_\mathrm{n} < 0$)—cf. [3], pp. 107 f., Eqs. (7.98), (7.99). In Eqs. (14), the coefficients $\tilde{a}_1$, $\tilde{a}_2$, and $\tilde{a}_2^*$ are constitutive parameters and may depend in principle on the temperature change $\left(\theta - \theta_0\right)$:

$$\tilde{a}_2 = \tilde{a}_{20}\left[1 + m_{\mathrm{a}2}\left(\theta - \theta_0\right)\right] \tag{15}$$

with the material parameters $\tilde{a}_{20}$ and $m_{\mathrm{a}2}$. The yield function $\tilde{f}$ and the plastic potential $\tilde{f}^*$ are depicted for the case of a fulfilled yield criterion at the reference temperature θ_0 and degree of cure $p = 1$ in Fig. 3—cf. [3], p. 108, Fig. 7.16. Both, the yield function and the plastic potential are elliptic for $\hat{t}_\mathrm{n} \geq 0$. If $\hat{t}_\mathrm{n} < 0$, the yield function changes into the DRUCKER-PRAGER-like criterion and the plastic potential to the VON MISES-like potential due to the MACAULAY bracket $\langle \hat{t}_\mathrm{n} \rangle$ in Eqs. (14). The rate of the plastic displacement jump $\dot{\boldsymbol{\Delta}}^{\mathrm{pl}}$ is derived from the plastic potential $(14)_2$ with the effective traction $\hat{\mathbf{t}}$ and the plastic multiplier λ:

$$\dot{\boldsymbol{\Delta}}^{\mathrm{pl}} = \lambda \frac{\partial\, \tilde{f}^*}{\partial\, \hat{\mathbf{t}}} = 2\,\lambda\left(\tilde{a}_2^* \left\langle \hat{t}_\mathrm{n} \right\rangle \mathbf{e}_\mathrm{n} + \hat{\tau}\, \mathbf{e}_\tau\right) \tag{16}$$

The strain equivalence principle leads to non-damaged plastic flow in the effective stress space, $\dot{\boldsymbol{\Delta}}^{\mathrm{pl}} = \dot{\hat{\boldsymbol{\Delta}}}^{\mathrm{pl}}$—cf. [3], p. 108. For the internal variable of the displacement-jump-type, $\dot{r}$ means the plastic arclength given by the EUCLIDean norm of the non-associated flow rule (16):

$$\dot{r} = \sqrt{\dot{\boldsymbol{\Delta}}^{\mathrm{pl}} \cdot \dot{\boldsymbol{\Delta}}^{\mathrm{pl}}} = 2\lambda \sqrt{\left(\tilde{a}_2^* \left\langle \hat{t}_\mathrm{n} \right\rangle\right)^2 + \hat{\tau}^2}\,, \tag{17}$$

cf. [3], p. 108 f. The yield stress τ_y in Eqs. (14) depends on the initial yield threshold $\tau_{\theta\mathrm{c}}$ and the stress of the nonlinear isotropic hardening R, which are both functions of the temperature θ and the degree of cure considering the thermal and chemical influence on the TAPO plasticity model. Furthermore, the nonlinear isotropic hardening part R is a function of the accumulated plastic arclength r:

$$\begin{aligned}
\tau_\mathrm{y} &= \tau_{\theta\mathrm{c}}(\theta, p) + R(r, \theta, p) \\
\tau_{\theta\mathrm{c}} &= \frac{\tau_0}{2}\left\{1 + \tanh\left[m_\tau\left(\theta_\tau - \theta\right)\right]\right\}\left(\frac{\left\langle p - p_\mathrm{gel}\right\rangle}{1 - p_\mathrm{gel}}\right)^{p_1} \\
R(r, \theta, p) &= \left\{q_\theta(\theta)\left[1 - \exp\left(-b_\theta(\theta)\, r\right)\right] + H_\theta(\theta)\, r\right\} \cdot \\
&\quad \cdot \left\{1 - \psi_1 \frac{1 - p}{1 - p_\mathrm{gel}}\right\}
\end{aligned} \tag{18}$$

The initial yield threshold $(18)_2$ is modelled with a hyperbolic-type function of temperature and a power function depending on the degree of cure following [26], p. 72. The temperature function is defined by means of the constitutive parameters τ_0, m_τ and θ_τ, whereas the function of cure is defined with the gel point p_gel and the exponent p_1. In contrast to [9] (pp. 203 f.), the parameters in the hardening part q_θ, b_θ, and H_θ are empirical, hyperbolic-type functions, which are well defined in the whole range of the absolute temperature $\theta \in [0, \infty)$:

$$\begin{aligned}
q_\theta(\theta) &= \frac{q_0}{2}\left\{1 + \tanh\left[m_q\left(\theta_q - \theta\right)\right]\right\} + q_1, \\
b_\theta(\theta) &= \frac{b_0}{2}\left\{1 + \tanh\left[m_b\left(\theta - \theta_b\right)\right]\right\} + b_1, \\
H_\theta(\theta) &= \frac{h_0}{2}\left\{1 + \tanh\left[m_h\left(\theta - \theta_h\right)\right]\right\} + h_1,
\end{aligned} \tag{19}$$

with the material parameters q_0, b_0, h_0, m_q, m_b, m_h, θ_q, θ_b and θ_h.

The influence of the degree of cure p on the hardening function $(18)_3$ is considered by a linear function with the material parameter ψ_1 and the gel point p_gel.

2.3 Temperature and cure dependent damage approach

A ductile damage approach is proposed for the TAPO model to predict damage due to the plastic deformation r, see [2], pp. 267 ff, [3], pp. 60 ff, and [4], p. 2-1157. In this contribution, the damage variable D is driven by the EUCLIDian norm of the vector for the mechanical displacement jump Δ^{vp}:

$$\begin{aligned}
D &= \left\langle \frac{\Delta^{\mathrm{vp}} - \Delta^{\mathrm{c}}}{\Delta^{\mathrm{f}} - \Delta^{\mathrm{c}}} \right\rangle^{n_\mathrm{D}}, \\
\dot{D} &= n_\mathrm{D} \left\langle \frac{\Delta^{\mathrm{vp}} - \Delta^{\mathrm{c}}}{\Delta^{\mathrm{f}} - \Delta^{\mathrm{c}}} \right\rangle^{n_\mathrm{D} - 1} \frac{\dot{\Delta}^{\mathrm{vp}}}{\Delta^{\mathrm{f}} - \Delta^{\mathrm{c}}}
\end{aligned} \tag{20}$$

with $\Delta^{\mathrm{vp}} = \sqrt{\boldsymbol{\Delta}^{\mathrm{vp}} \cdot \boldsymbol{\Delta}^{\mathrm{vp}}}$ and $\boldsymbol{\Delta}^{\mathrm{vp}} = \boldsymbol{\Delta}^{\mathrm{ve}} + \boldsymbol{\Delta}^{\mathrm{pl}}$. The damage evolution $(20)_2$ is controlled by the exponent n_D, the critical Δ^{c}, and the displacement jump Δ^{f} at failure. In detail, Δ^{c} describes the displacement jump at damage initialisation (tensile strength) and Δ^{f} is the displacement jump at failure of the adhesive in the sense to the approach of JOHNSON and COOK in [27]. Both, Δ^{c} and Δ^{f} are functions of the stress ratio

$$T = \left\langle \hat{t}_\mathrm{n} \right\rangle \Big/ \sqrt{\hat{t}_\mathrm{n}^{\,2}/3 + \hat{\tau}} \tag{21}$$

according to [3], p. 109. The thermal influence on damage is included by the functions for Δ^{c} and Δ^{f} according to JOHNSON and COOK [27]. The influence of the degree of cure is considered with two different power functions in Δ^{c} and Δ^{f}:

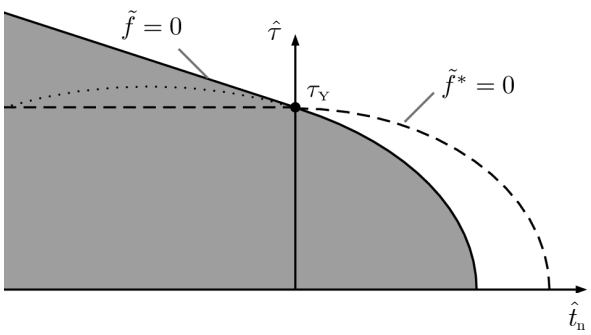

Fig. 3 Yield function $\tilde{f}$ and plastic potential $\tilde{f}^*$ in $\hat{t}_\mathrm{n}$ - $\hat{\tau}$ -diagram at θ_0—cf. [3], p. 108

$$\Delta^{\mathrm{c}} = \left[d_{\mathrm{I1}} + d_{\mathrm{I2}} \exp\left(-d_3 \left\langle T \right\rangle\right)\right] \left\langle 1 + m_{\mathrm{f}} \left(\theta - \theta_0\right)\right\rangle \cdot \left[1 - \left(\frac{1-p}{1-p_{\mathrm{gel}}}\right)^{\beta_1}\right],$$
$$\Delta^{\mathrm{f}} = \left[d_1 + d_2 \exp\left(-d_3 \left\langle T \right\rangle\right)\right] \left\langle 1 + m_{\mathrm{f}} \left(\theta - \theta_0\right)\right\rangle \cdot \left[1 - \delta_1 \left(\frac{1-p}{1-p_{\mathrm{gel}}}\right)^{\delta_2}\right] \quad (22)$$

with the constitutive parameter m_{f} and the room temperature θ_0 for the temperature dependency and the constitutive parameters β_1, δ_1, and δ_2 for the cure dependency. Thus, the parameters d_{I1}, d_{I2}, d_1, d_2, and d_3 are related to the fully cured adhesive with $p = 1$ at room temperature θ_0.

2.4 Implementation

Finally, the constitutive equations shown are implemented into the FE software LS-DYNA as a user defined cohesive model for the eight node cohesive zone element—see [4], pp. 2-264 ff. Therefore, the thermo-viscoelastic convolution integral is numerically integrated with the recursive, implicit, one step algorithm by TAYLOR et al. [28] and solved with the equations of the TAPO plasticity model by the predictor corrector scheme. Also, the consistent tangent modulus is derived and implemented into LS-DYNA for the quasi-static FE analysis of the long-term behaviour of adhesive bonds.

3 Parameter identification and verification

The parameters of the nonlinear evolution equation for the degree of cure (5) and the ARRHENIUS equations (6) are identified with test data measured in the Differential Scanning Calorimetry (DSC) with a bulk specimen of the adhesive BETAMATE 1496V by DOW Automotive [29] at the Laboratory for Material and Joining Technology (LWF) at the University of Paderborn. In rheometer tests, the gel point p_{gel} is identified with the temperature at the local maximum of the loss angle measured for the curing adhesive at the LWF. Also, the parameters of the thermo-viscoelastic model are identified by means of tests with bulk specimens of the adhesive using the Dynamic Mechanical Analysis (DMA) at the LWF. The DMA tests are conducted in bending and shear mode to identify the DIRICHLET-PRONY series of the elastic $E(t,\theta)$ and shear modulus

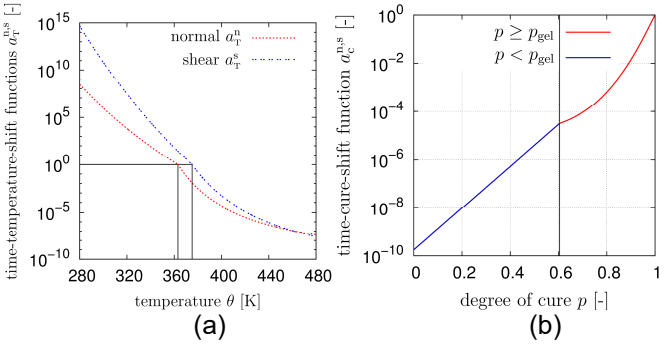

Fig. 4 (a) time-temperature shift functions (LWF), (b) time-cure-shift function

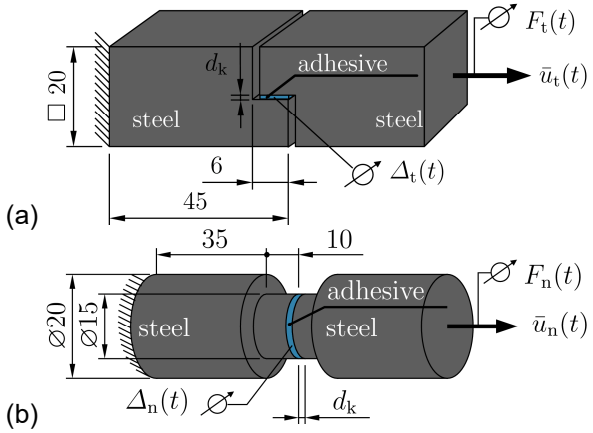

Fig. 5 TASS (a) and BJS (b) with geometrical dimensions in [mm], see [9], p. 13-14, (LWF)

$G(t,\theta)$ in time t and temperature θ by the time-temperature shift. Here, the elastic parameters $E(t,\theta)$ and $G(t,\theta)$ are approximately used for the interface stiffness in the normal and tangential direction (11) with the layer thickness d_{k} as follows:

$$E(t,\theta)/d_{\mathrm{k}} \approx R_{\mathrm{n}}(t,\theta) + k_{\infty}\ ,\ G(t,\theta)/d_{\mathrm{k}} \approx R_{\mathrm{s}}(t,\theta) + g_{\infty} \quad (23)$$

The time-temperature-shift functions $a_{\mathrm{T}}^{\mathrm{n}}(\theta(t))$ and $a_{\mathrm{T}}^{\mathrm{s}}(\theta(t))$ are identified at the LWF empirically by shifting the complex moduli of different isothermal temperature states along the frequency axis to obtain a single smooth master curve. The bending mode provides the time-temperature-shift functions for the normal direction and the shear mode comprises the shift function for the tangential direction of the interface—see Eqs. (8). Therefore, the ARRHENIUS and WILLIAMS-LANDEL-FERRY equations (8) are fitted to the test data of the time-temperature shift along the temperature axis in Fig. 4 (a). The time-cure-shift function (9) is fitted to the data of DMA tests with different degrees of cure conducted at the LWF. The resultant time-cure-shift function is plotted in Fig. 4 (b).

Tests with the thick adherend shear specimen (TASS) and the butt joint specimen (BJS) are conducted at the LWF for different constant temperature states and different degrees of cure beyond the gel point in [9], pp. 46-71 and the current FOSTA project P 1087, respectively. The TASS consists of two prismatic steel

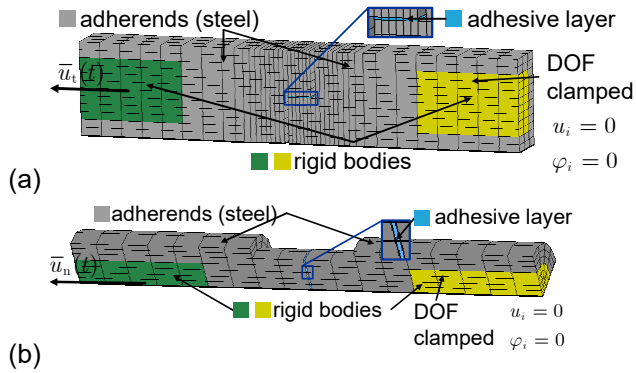

Fig. 6 FE model of the TASS (a) and the BJS (b) with part declaration and boundary conditions

adherends bonded by an adhesive with constant layer thickness $d_\mathrm{k} = 0.3$ mm and an overlap of 5 mm in the stepped region—see Fig. 5 (a) and [9], p. 13. In the test, the adhesive layer is sheared by moving one of the adherends in the direction tangential to the plane of the adhesive layer with the time-displacement course $\overline{u}_\mathrm{t}(t)$, while the other one is clamped. During the test, the relative displacement between the adherends $\Delta_\mathrm{t}(t)$ is controlled to ensure the nominal shear rate $\tan\dot{\gamma} = \dot{\Delta}_\mathrm{t} \,/\, d_\mathrm{k} = 2.0 \cdot 10^{-3}\ \mathrm{s}^{-1}$. The resulting force $F_\mathrm{t}(t)$ is measured by a load cell at one of the clamps of the specimen.

The test provides the measured data of the relative displacement between the adherends $\Delta_\mathrm{t}(t)$ and the related force $F_\mathrm{t}(t)$. The butt joint specimen consists of two cylindrical, stepped steel adherends, which are bluntly bonded by an adhesive with the same layer thickness as defined above—see Fig. 5 (b) and [9], p. 14. Again, One of the adherends is fixed and the other one is displaced normal to the plane of the adhesive layer with the time-displacement course $\overline{u}_\mathrm{n}(t)$. The relative displacement between the adherends $\Delta_\mathrm{n}(t)$ is monitored to force a nominal strain rate of $\dot{\varepsilon} = \dot{\Delta}_\mathrm{n} \,/\, d_\mathrm{k} = 2.0 \cdot 10^{-3}\ \mathrm{s}^{-1}$ throughout the test. Hence, the test provides the measured data of the relative displacement between the adherends $\Delta_\mathrm{n}(\mathrm{t})$ and the related force $F_\mathrm{n}(t)$ of the load cell versus time.

The FE models take advantage of the symmetry of the specimens in order to reduce the number of elements and nodes—see Fig. 6. The adherends are meshed with solid elements and the adhesive layer is modelled with cohesive elements in both FE models. For the steel adherends, the isotropic hypoelastic material model, suitable for large rotation and small strains, is used with the elastic modulus $E_\mathrm{st} = 210000\ \mathrm{N/mm^2}$ and the Poisson ratio $\mu_\mathrm{st} = 0.3$—see [4], p. 2-64. The density is set to $\delta_\mathrm{st} = 7850\,\mathrm{kg/m^3}$ on the material card. Moreover, the temperature dependent TAPO model is invoked to describe the behaviour of the adhesive bond for the cohesive elements.

The adherends of the specimens are connected with the clamps of the tensile testing machine by screws in the test setups. For simplicity, the screws in the adherends are modelled with rigid bodies as shown in the FE models in Fig. 6. The time-displacement courses of the tests are prescribed for the green rigid bodies, whereas the yellow rigid bodies are clamped in order to disable all translational u_i and rotational φ_i degrees of freedom (DOF). Also, adequate boundary conditions are prescribed in the symmetry planes of both specimens.

In a second identification step, the instantaneous stiffness parameters $k_0 = k_\infty + \sum_i k_i$ and $g_0 = g_\infty + \sum_i g_i$ of the DIRICHLET-PRONY series are fitted to the first slope of the data in Fig. 7 (a) and (b) measured in the tests with the TASS and BJS to accomplish the stiffness of the adhesive bond. Here, the participation factors $\nu_i^\mathrm{n} = k_i/k_0$, $\nu_\infty^\mathrm{n} = k_\infty/k_0$ and $\nu_i^\mathrm{s} = g_i/g_0$, $\nu_\infty^\mathrm{s} = g_\infty/g_0$ are kept constant between the instantaneous stiffness parameters k_0, g_0 and the stiffness parameters of the individual MAXWELL chains k_i, g_i and the equilibrium stiffness k_∞ and g_∞. Also, the material parameters of the time-cure shift function $a_\mathrm{gel}^\mathrm{n,s}$, $a_1^\mathrm{n,s}$, and $a_2^\mathrm{n,s}$ are adapted to the first slope of the data recorded in tests with the TASS and BJS at the LWF in Fig. 7 (c) and (d) for different degrees of cure in the range from the gel point $p = p_\mathrm{gel}$ to the fully cured state $p = 1$.

Furthermore, the thermoplastic and damage parameters are inversely identified by fitting the model response of the FE simulation to the related test data of the TASS and the BJS in Fig. 7. The result of the identification is added to Fig. 7 comparing the data of the FE result to the test data for the performance of the model in the verification step for different temperature and cure states. It can be observed, that the actual yield stress in tension and shear strength steadily decrease with rising temperature or decreasing degree of cure, whereas the critical strain at the shear strength increases in temperature and degree of cure. In the FE simulation, the traction is dominated by the overstress in the MAXWELL elements for the quasi-static loading in both test series due to the small equilibrium stiffness k_∞ and g_∞.

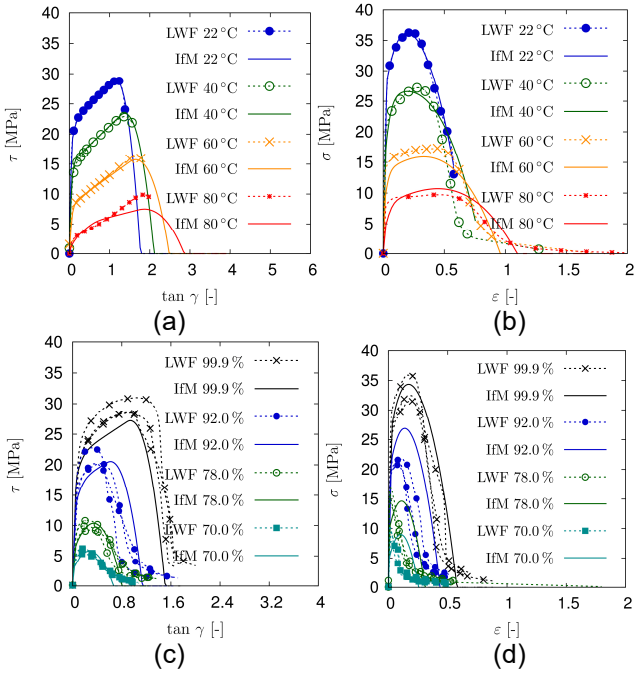

Fig. 7 Comparison of test data by the LWF (lines with symbols) and model response (dashed dotted and solid lines) with identified parameters: (a) and (b) TASS and BJS with cured adhesive at different temperatures, (c) and (d) TASS and BJS with different degrees of cure at room temperature

4 Model validation

A bimetallic specimen is tested at the LWF in Paderborn for the purpose of validation—see [9], pp. 237 ff. It consists of an aluminium and a steel sheet strip with different thermal expansion coefficients $\alpha_\mathrm{al}^\mathrm{th} = 2.4 \cdot 10^{-5}\ \mathrm{K}^{-1}$ and $\alpha_\mathrm{st}^\mathrm{th} = 1.3 \cdot 10^{-5}\ \mathrm{K}^{-1}$, respectively. For the steel sheet strip, the material parameters are the elastic modulus $E_\mathrm{st} = 210000\ \mathrm{N/mm^2}$ and

the Poisson ratio $\mu_{st} = 0.3$, whereas the parameters of the aluminium strip are taken as $E_{al} = 70000\ \mathrm{N/mm^2}$ and $\mu_{al} = 0.34$. The densities of the steel and aluminium sheet are set to $\delta_{st} = 7850\,\mathrm{kg/m^3}$ and $\delta_{al} = 2700\,\mathrm{kg/m^3}$. Both strips are joined with the cured, thermosetting, ductile-modified, structural adhesive BETAMATE 1496V at the right hand side and clamped at the left hand side as shown in Fig. 8 (a). In the second setting, the adhesive between the strips is uncured. In both test settings, the specimen is heated in the oven to achieve a temperature induced thermal expansion of the sheet metals, leading to shear deformations in the adhesive. The bimetallic specimen is tested to investigate the displacement due to bending and shearing of the adhesive under arbitrary thermal loading. The deflection u_z at the tip and the relative displacement between the sheets at the adhesive bond Δu_x are measured with an optical device under a typical time-temperature loading.

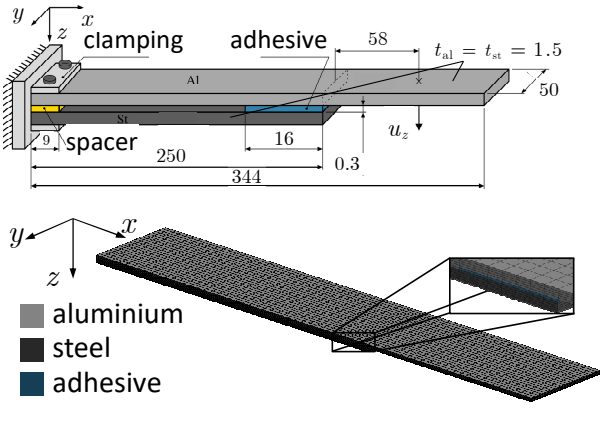

Fig. 8 (a) scheme of the bimetallic specimen in [9], pp. 14 ff, with dimensions in [mm] and (b) FE model of the bimetallic specimen

In the first setting, the specimen is linearly heated up from nearly room temperature to about 81 °C within 6 min, followed by a hold time at about 81 °C for 125 min and an uncontrolled cooling process up to nearly room temperature as shown in Fig. 9 (a). In the second setting, the adhesive is cured during the tests in the oven. Here, the bi-metal specimen is heated up to the cure temperature of 180 °C held for about 36 min followed by an uncontrolled cooling process as shown in Fig. 9 (b).

Finally, the test data of the bimetallic specimen are compared to the data of the related FE simulation for the validation of the constitutive equations of the temperature dependent TAPO model—cf. [9], pp. 255 ff. The bimetallic specimen is simulated with the FE-program LS-DYNA [30]. In the FE model as in Fig. 8 (b), both sheets are spatially discretised by means of the enhanced solid element and characterised with the isotropic hypoelastic material model. The isotropic thermal expansion is taken into account for both sheets. The adhesive is discretised using the

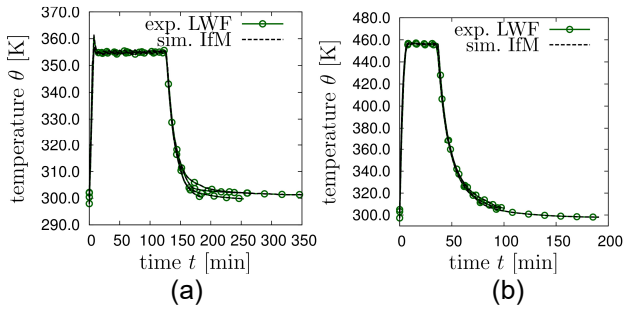

Fig. 9 Time-temperature-course of the bi-metal specimens with (a) fully cured and (b) uncured adhesive layers—see [9]

cohesive element and is described by the extended TAPO model as a “user defined cohesive model”. A node to node connection is used between the cohesive and the solid elements. The measured time-temperature-courses of the bimetallic tests are prescribed to the nodes by means of a thermal load curve on the assumption of a homogeneous temperature distribution across the specimen. For simplification, the clamp of the bimetallic specimen is not modelled in detail. Rather, a set of boundary conditions is used to fix the sheets in space and allow thermal expansions at the clamp to prevent artificial stresses in the sheets. In the test setup, a spacer ensures the distance between the sheets at the clamp, see Fig. 8. Therefore, the DOF in z-direction are fixed for the nodes at the bottom of the aluminium and the top of the steel sheet in the area of the clamp. Fig. 10 (a) shows the data of the tip deflection u_z of the four tests with the cured adhesive, which are in the range from 8 mm to 10 mm at the end of the heating process. During the state of constant temperature, they decrease to approximately 6 mm to 8 mm because of stress relaxation towards the equilibrium stress in the adhesive. Furthermore, u_z declines below its initial value after cooling down to room temperature.

In Fig. 10 (b), the test data of the relative displacement Δu_x of the cured bi-metal specimen are plotted versus time t. During the heating process, Δu_x increases to approximately constant values between 0.09 mm and 0.1 mm. After cooling down the specimen, Δu_x decreases nearly to the initial value.

The test data of the deflection u_z for the bi-metal specimen with the initially uncured adhesive are shown in Fig. 10 (c). Here, the values of the deflections are only significant in the cooling process, which is expected after the curing process. In the test data, there is an unexpected negative and positive deflection during the temperature is held constant.

The relative displacement is shown in Fig. 10 (d). Here, the courses of the test data are almost similar to the curves in Fig. 10 (b). The maximum of the relative displacement is much higher than the curves in Fig. 10 (b) because the stiffness of the uncured adhesive is much lower than the stiffness of the fully cured.

Finally, the deflection at the tip u_z and the relative displacement Δu_x of the FE simulation are compared to the test data in Fig. 10 (a) to (d). As a result, the computed deflection at the tip u_z is in the range of the scatter band of the measured test data for both test settings as shown in Fig. 10 (a) and (c). The relative displacement Δu_x in Fig. 10 (b) is in a good agreement with the test data, whereas there is a significant gap for Δu_x between the data of the tests and simulation in Fig. 10 (d) after the cooling process.

5 Summary and Outlook

The temperature dependent TAPO cohesive model is presented describing thermo-viscoelastic phenomena before and thermo-plasticity beyond the yield threshold. Also, the material model takes temperature dependent damage up to failure into account. The constitutive parameters are identified by fitting the model response of the FE simulation to the related test data of the TASS and the BJS. Furthermore, the constitutive equations are verified by the FE simulation of the tests with the TASS and BJS. Finally, the material model is validated with bimetallic tests by comparing the FE simulation to the measured data in the test. The stress relaxation is indirectly evaluated through the deflection at the tip u_z and the relative displacement between the sheets Δu_x with respect to temperature, deformation, and time by means of the bimetallic specimen. In summary, the constitutive model successfully predicts the test results of the bimetal specimen for both test setups. As a result, the mechanical properties of the adhesively bonded joint

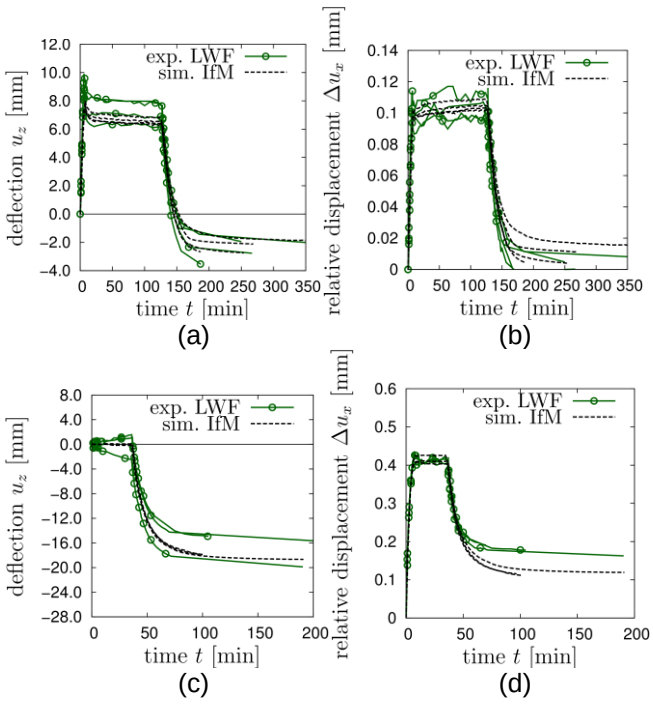

Fig. 10 Validation of (a) tip deflection u_z and (b) relative displacement Δu_x of fully cured adhesive and (c) tip deflection u_z and (d) relative displacement Δu_x during cure in bimetal specimen—cf. [9], pp. 259 ff for (a) and (b).

depend on temperature and degree of cure heavily. Further test have to be performed in order to proof the validity of the proposed constitutive model. In particular, future test setups must exhibit failure of the adhesive bond during service and manufacturing loads.

6 Acknowledgement

We thankfully acknowledge financial support of the Federal Ministry for Economic Affairs and Energy through the AiF (Arbeitsgemeinschaft industrieller Forschungsvereinigungen "Otto von Guericke" e.V.) by grant P 1087 / 18895 N of the FOSTA—Forschungsvereinigung Stahlanwendung e.V., Sohnstr. 65, 40237 Düsseldorf, Germany.

7 References

[1] Schlimmer, M., Barthel, C., Pauli, J., Siebert, M., Matzenmiller, A., Fiolka, M., Gerlach, S., Mahnken, R., Hentrich, M., Hahn, O., Jendrny, J., Wißling, M., Dilger, K., Welters, T., Gumbsch, P., Andrieux, F., Memhard, D., Sun, D.-Z., Thoma, K., Nossek, M., Sauer, M., Hennemann, O.-D., Brede, M. (ed.), Hesebeck, O. and Marzi, S.: *Forschung für die Praxis P 676: Development of Methods to Simulate High Strength Adhesive Joints with Sheet Steel at Crash Conditions for Vehicle Construction*. Report of project P 676, Forschungsvereinigung Stahlanwendung e. V., Sohnstraße 65, 40237 Düsseldorf: Verlag und Vertriebsgesellschaft mbH, Düsseldorf, 2008. Download author-created version.

[2] Brede, M., Hesebeck, O. (eds.), Marzi, S., Mahnken, R., Nörenberg, N., May, M., Kilchert, S., Voß, H., Matzenmiller, A., Burbulla, F., Memhard, D., Böhme, W., Lienhard, J., Fehrenbach, C. and Reissig, L.: *Robustness and Reliability of Methods to Simulate Adhesive Joints with High Strength Steel Sheets at Crash Conditions*. Report of project P 828, Forschungsvereinigung Stahlanwendung e. V., Sohnstr. 65, 40237 Düsseldorf, in press. Download author-created version.

[3] Burbulla, F.: *Kontinuumsmechanische und bruchmechanische Modelle für Werkstoffverbunde*, PhD thesis, Institute of Mechanics, Department of Mechanical Engineering, University of Kassel, 2015.

[4] Livermore Software Technology Corporation (LSTC): LS-DYNA keyword user´s manual – volume II – Material Models – 03/23/15. Livermore, California, USA, 2015.

[5] Matzenmiller, A. and Burbulla, F.: Kontinuumsmechanische Modellierung von Stahlblechklebverbindungen für die FE-Crashanalyse, *Proceedings of the 7th LS-DYNA Forum*, 2008, Bamberg, DYNAmore GmbH, Stuttgart, 2008. [PDF]

[6] Gerlach, S., Fiolka, M. and Matzenmiller, A.: Modelling and analysis of adhesively bonded joints with interface elements for crash analysis, *Proceedings of the 4th LS-DYNA Forum*, 2005,

Bamberg, DYNAmore GmbH, Stuttgart, 2005. [PDF]

[7] Matzenmiller, A., Gerlach, S. and Fiolka, M.: Progressive Failure Analysis of Adhesively Bonded Joints in Crash Simulations, *Proceedings of the 5th LS-DYNA User Forum*, 2006, Ulm, DYNAmore GmbH, Stuttgart, 2006. [PDF]

[8] Matzenmiller, A., Gerlach, S. and Fiolka, M.: A critical analysis of interface constitutive models for the simulation of delamination in composites and failure of adhesive bonds, *Journal of Mechanics of Materials and Structures*, vol. 5 (2), pp. 185-211, 2010.

[9] Meschut, G., Teutenberg, D. (ed.), Lion, A., Liebl, C., Matzenmiller, A. and Kühlmeyer, P. (ed.): *Development of Methods for Simulation and Evaluation of Damage in Adhesive Layers due to Thermal Cyclic Loadings during Manufacturing and Operation*. Report of project P 878, Forschungsvereinigung Stahlanwendung e. V., Sohnstr. 65, 40237 Düsseldorf, in press. Download author-created version.

[10] Liebl, C.: *Viskoelastisch-viskoplastische Modellierung von Strukturklebstoffen während der Aushärtung*, PhD thesis, Institute of Mechanics, Faculty of Aerospace Engineering, Munich University of the Federal Armed Forces, 2014.

[11] Enns, J.B. and Gillham, J.K.: Time-Temperature-Transformation (TTT) Cure Diagram: Modeling the Cure Behavior of Thermosets. *Journal of Applied Polymer Science*, 28, pp. 2567–2591, 1983.

[12] Kamal, M. R.: Thermoset Characterization for Moldability Analysis. *Polymer Engineering and Science*, 14(3), S. 231–239, 1974.

[13] Kamal, M. R. and Sourour, S.: Kinetics and Thermal Characterization of Thermoset Cure. *Polymer Engineering and Science*, 13(1), S. 59–64, 1973.

[14] Schwarzl, F.R., Staverman, A.J.: Time-Temperature Depandence of Linear Viscoelastic Behavior. *Journal of Applied Physics*. 23(8), 838–843, 1952.

[15] Ferry, J.D.: *Viscoelastic Properties of Polymers*, John Wiley & Sons, 3rd Edition, 1980.

[16] Schwarzl, F. R.: *Polymermechanik, Struktur und mechanisches Verhalten von Polymeren*, Springer-Verlag, 1990.

[17] Adolf, D. and Martin, J. E.: Time-Cure Superposition during Cross-Linking. *Macromolecules*, 23(15), S. 3700–3704, 1990.

[18] Adolf, D. and Martin, J. E.: Calculation of Stresses in Crosslinking Polymers. *Journal of Composite Materials*, 30(13), S. 13–34, 1996.

[19] Christensen, R. M.: Theory of Viscoelasticity, An Introduction, Academic Press, 1982.

[20] Williams, M. L. ,Landel, R. F. and Ferry, J. D.: The Temperature Dependence of Relaxation Mechanisms in Amorphous Polymers and Other Glassforming liquids. *Journal of the American Chemical Society*, 77(14), S. 3701–3707, 1955.

[21] Eom, Y., Boogh, L., Michaud, V., Sunderland, P. and Manson, J.-A.: Time-Cure-Temperature Superposition for the Prediction of Instantaneous Viscoelastic Properties During Cure. *Polymer Engineering and Science*, 40(6), S. 1281–1292, 2000.

[22] Matzenmiller, A., Kurnatowski, B., Hanselka, H., Bruder, T., Schmidt, H., Mayer, B., Schneider, B., Kehlenbeck, H., Nagel, C. and Brede, M. (ed.): *Design of Adhesive Joints with Steel Components at Loading with Variable Amplitudes for Vehicle Construction*. Report of project P 796, Forschungsvereinigung Stahlanwendung e. V., Sohnstr. 65, 40237 Düsseldorf, 2012. Download author-created version.

[23] Kachanov, L. M.: Rupture time under creep conditions. *International Journal of Fracture*, vol. 97, pp. 11-18, 1999. Translated from Izvestia Akademii Nauk SSSR, Otdelenie tekhnicheskich nauk, vol. 8, pp. 26-31, 1958, in Russian.

[24] Rabotnov, Y. N.: On the equations of state of creep. *Proceedings of the Institution of Mechanical Engineers*, Conference Proceedings, vol. 178, pp. 2-117-2-112, 1963.

[25] Bröcker, C. and Matzenmiller, A.: Thermomechanically consistent material modeling with damage for simultaneous hot/cold forming based on enhanced rheological models. J. Eberhardsteiner, H. Böhm and F. Rammerstorfer (eds.): *Proc. of 6th European Congress on Computational Methods in Applied Sciences and Engineering (ECCOMAS).* Vienna Universtity of Technology, Austria, 2012.

[26] Menzel, S.: *Zur Berechnung von Klebverbindungen hybrider Karosseriestrukturen beim Lacktrocknungsprozess*. PhD thesis, Institut für Leichtbau und Kunststofftechnik, Fakultät für Maschinenwesen, Technische Universität Dresden, 2011.

[27] Johnson, G. R., Cook, W. H.: Fracture characteristics of three metals subjected to various strains, strain rates, temperatures and pressures. *Engineering Fracture Mechanics*, vol. 21, pp. 31-48, 1985.

[28] Taylor, R. L., Pister, K. S., Goudreau, G. L.: Thermomechanical analysis of viscoelastic solids. *International Journal for Numerical Methods in Engineering*, vol. 2, pp. 45-59, 1970.

[29] Dow Automotive: Techincal Datasheet BETAMATE 1496 V. Issue 10, 04.06.2007. Dow Automotive (Deutschland) GmbH, 65824 Schwalbach, 2007.

[30] Livermore Software Technology Corporation (LSTC): LS-DYNA keyword user´s manual – volume I – 03/23/15. Livermore, California, USA, 2015.

8 Appendix

8.1 Material parameter of the thermo-chemo-viscoelastic part of the constitutive model

Tab. 1 DIRICHLET-PRONY series tangential to interface

R_{s} tangential			
i	$\nu_i^{\mathrm{s}} = g_i / g_0$	$g_i \left[\frac{\mathrm{MPa}}{\mathrm{mm}}\right]$	$\hat{\tau}_i^{\mathrm{s}} [\mathrm{s}]$
1	0.17285	288.45	6.58E-07
2	0.17996	300.31	9.85E-06
3	0.16406	273.78	1.37E-04
4	0.16656	277.95	1.87E-03
5	0.15599	260.31	2.40E-02
6	0.10370	173.05	2.80E-01
7	0.03769	62.89	2.88E+00
8	0.01047	17.46	3.78E+01
9	0.00257	4.28	1.02E+03
g_∞	0.00618	10.31	-
g_0	-	1668.79	-

Tab. 2 Dirichlet-Prony series normal to interface

R_{n} normal			
i	$\nu_i^{\mathrm{n}} = k_i / k_0$	$k_i \left[\frac{\mathrm{MPa}}{\mathrm{mm}}\right]$	$\hat{\tau}_i^{\mathrm{n}} [\mathrm{s}]$
1	0.16600	1476.36	6.03E-14
2	0.05470	486.49	6.29E-12
3	0.06460	574.53	9.94E-13
4	0.05720	508.72	3.96E-11
5	0.05340	474.93	2.65E-10
6	0.04970	442.02	1.57E-09
7	0.04700	418.01	8.78E-09
8	0.04810	427.79	4.59E-08
9	0.04270	379.76	2.10E-07
10	0.05120	455.36	8.43E-07
11	0.06850	609.22	5.45E-06
12	0.07670	682.15	5.01E-05
13	0.07510	667.92	6.36E-04
14	0.06260	556.75	8.01E-03
15	0.03780	336.18	6.96E-02
16	0.01710	152.08	3.65E-01
17	0.01080	96.05	1.45E+00
18	0.00685	60.92	7.22E+00
19	0.00327	29.08	4.72E+01
20	0.00128	11.38	2.80E+02
21	0.00054	4.80	1.29E+03
22	0.00029	2.59	6.28E+03
23	0.00013	1.14	4.02E+04
24	0.00006	0.57	1.51E+05
k_∞	0.00429	38.15	-
k_0	-	8892.95	-

Tab. 3 Time-temperature/time-cure shift functions

normal direction (LWF)			
$C_1^{\mathrm{n}} [-]$	$C_2^{\mathrm{n}} [\mathrm{K}]$	$E_{\mathrm{A}}^{\mathrm{n}} [\mathrm{K}]$	$\theta_{\mathrm{R}}^{\mathrm{n}} [\mathrm{K}]$
29.63	72.5	37301.8	375.15
tangential direction (LWF)			
$C_1^{\mathrm{s}} [-]$	$C_2^{\mathrm{s}} [\mathrm{K}]$	$E_{\mathrm{A}}^{\mathrm{s}} [\mathrm{K}]$	$\theta_{\mathrm{R}}^{\mathrm{s}} [\mathrm{K}]$
25.14	55.6	23739.65	363.15
Time-cure shift function			
$a_{\mathrm{gel}}^{\mathrm{n,s}}$	$a_1^{\mathrm{n,s}}$	$a_2^{\mathrm{n,s}}$	$a_3^{\mathrm{n,s}}$
10.3668	7.005	1.0666	8.0

8.2 Material parameter of the thermo-chemo-plastic part of the constitutive model

Tab. 4 Thermo-chemo-plastic material parameters

$\tau_0 [\mathrm{MPa}]$	$m_\tau \left[\mathrm{K}^{-1}\right]$	$\theta_\tau [\mathrm{K}]$	$\theta_0 [\mathrm{K}]$
42.18	0.0187811	288.8	295.15
$q_0 [\mathrm{MPa}]$	$m_q \left[K^{-1}\right]$	$\theta_q [\mathrm{K}]$	$q_1 [\mathrm{MPa}]$
1.91557	0.103464	321.83	1.90707
$b_0 \left[\mathrm{mm}^{-1}\right]$	$m_b \left[K^{-1}\right]$	$\theta_b [\mathrm{K}]$	$b_1 \left[\mathrm{mm}^{-1}\right]$
135.618	0.124202	312.97	44.0779
$h_0 \left[\frac{\mathrm{MPa}}{\mathrm{mm}}\right]$	$m_h \left[K^{-1}\right]$	$\theta_h [\mathrm{K}]$	$h_1 \left[\frac{\mathrm{MPa}}{\mathrm{mm}}\right]$
0.0	0.0	0.0	22.895
p_1		ψ_1	
1.22836		0.38794801	
$\tilde{a}_1$	$\tilde{a}_{20}$	$\tilde{a}_2^*$	$m_{a2} \left[K^{-1}\right]$
0.4457	0.1249	0.3383	0.0109701

8.3 Material parameters of the temperature and cure dependent ductile damage model

Tab. 5 Material parameters for ductile damage with temperature and cure dependency

$d_{\mathrm{I1}} [\mathrm{mm}]$	$d_{\mathrm{I2}} [\mathrm{mm}]$	$d_1 [\mathrm{mm}]$	n
0.279E-3	0.3304	0.2065	2.0
$d_2 [\mathrm{mm}]$	$d_3 [-]$	$m_{\mathrm{f}} \left[K^{-1}\right]$	
0.3314	6.935	0.01054	
β_1	δ_1	δ_3	
0.4662	0.6961	0.4130	

8.4 Degree of cure

Tab. 6 Parameters of nonlinear evolution equation for degree of cure, ARRHENIUS equations and gel point (LWF)

m	n_1	n_2	p_{gel}
1.3193	0.7620	2.3298	0.6044
$\log A_{10}$	$\log A_{20}$	$E_1 \left[\frac{\mathrm{kJ}}{\mathrm{mol}}\right]$	$E_2 \left[\frac{\mathrm{kJ}}{\mathrm{mol}}\right]$
7.8337	9.0235	91.9443	88.30247